Ion bombardment of reconstructed metal surfaces: From two-dimensional dislocation dipoles to vacancy pits

O. Rodríguez de la Fuente,* M. A. González, and J. M. Rojo
Departamento de Física de Materiales, Universidad Complutense, 28040 Madrid, Spain
(Received 3 May 2000; revised manuscript received 19 September 2000; published 8 February 2001)

By means of scanning tunnel microscopy the surface morphology of reconstructed Au(001) surfaces has been studied after bombardment with 600 eV Ar ions as a function of dose, in the range of 10^{13} to 10^{16} ions/cm^2, and the experimental results analyzed in the light of molecular dynamics simulations using a *glue* potential. At low dose (5×10^{13} ions/cm^2) new defects, different from the commonly observed vacancy islands are reported. They appear as *depressions* 0.06 nm deep, with a characteristic width of 1.44 nm. Bombardment with similar doses of Pt(001) show the same general behavior. Molecular dynamics simulations with a realistic *glue* potential that reproduces the hexagonal-like Au(001) reconstruction, confirm that these *depressions* are in fact two-dimensional $\pi/3$ dislocation dipoles originated by the relaxation of vacancy rows on the ridges of the topmost reconstructed layer. These two-dimensional dipoles are seen to dissociate into individual two-dimensional dislocations that display the characteristics of ordinary bulk dislocations, e.g. glide or climb. At higher doses ($\simeq3\times10^{14}$ ions/cm^2), but well below a nominal removal of 1 monolayer, vacancy islands, one atomic spacing high, are seen to nucleate on these *depressions*. With increasing ion damage these vacancy islands become the dominant feature. For doses of about 10^{15} ions/cm^2, other defects related to the reconstruction, such as perpendicular reconstruction domains and unreconstructed patches of (001) square symmetry, become visible.

DOI: 10.1103/PhysRevB.63.085420 PACS number(s): 68.35.Bs, 68.35.Fx, 68.35.Dv, 61.80.Jh

I. INTRODUCTION

It is well known that crystal defects influence bulk physical properties of solid materials, the analysis of their behavior being an essential chapter of solid state physics. Bulk defects are routinely characterized by a number of well-developed experimental techniques, such as electrical resistivity measurements or transmission electron microscopy.[1] These techniques have been applied to the study of point (vacancies and interstitials), line (dislocations), or two-dimensional (stacking faults and grain boundaries) defects. The resulting empirical knowledge, along with parallel theoretical work, allows us to establish a good correlation between the observed variations in the physical properties and specific bulk defects.

A completely different picture arises in regard to *surface defects*, particularly in metals. Surface defects are believed to exert a great influence on a number of important processes in which surfaces play a major role, such as corrosion and catalysis.[2] Nevertheless, with the exception of steps, very little can be stated even about the simplest properties of such surface defects. For example, the value of the migration energy for vacancies on a surface is largely a controversial issue.[3] This is a serious drawback because in some metal surfaces[4] vacancy diffusion has been claimed to be the controlling mechanism for mass transport and other important surface processes. In the case of more complex defects, such as vacancy islands or dislocation configurations, reliable data are particularly scarce. No doubt, the lack in the past of experimental techniques sensitive to surface defects has contributed to this situation. More recently, the development of the scanning tunneling microscope (STM) has opened the possibility of studying surfaces and their defects with unprecedented resolution.[5–16] Provided that the surface is not too rough, this real-space method gives topographic and structural information on a subnanometer scale, which can lead to an atomic-scale description of surface defects.

To study surface defects, a controlled procedure of defect creation is desirable. For this purpose ion bombardment may be advantageous since (a) the density of defects depends on the dose (number of ions impinging per unit surface area) and (b) the nature of the primary damage depends also on ion energy. It is known[12–16] that when a metal surface is irradiated with ions with energies up to a few keV in the low- and medium-dose regimes (less than 0.5 ions per surface atom), only vacancies and adatoms are generated; they may subsequently cluster. At higher ion energies, in addition to those point defects, a primary damage in the form of dislocation loops (that can intersect the surface) can also be created in the near-surface region as a consequence of the collapse of vacancy-rich nuclei of displacement cascades.[17] One can see that by judicious choice of irradiation parameters a wide selection of conditions can be reached.

In addition to its role as a controlled source of surface defects, ion-beam irradiation has recently become an issue of increasing scientific and technological interest in regard to the possibility of controlled modification of surfaces. Low-energy ion bombardment has been used during film growth as a mean to lower deposition temperatures and to improve certain film properties.[18] In experiments in which the ion energies are typically kept below 100 eV, the main effect of ions is to increase surface diffusion,[19] favoring layer-by-layer two-dimensional (2D) growth. Although higher ion energies may damage the film due to defect formation or substrate sputtering, it has been reported[20] that pulses of 600 eV Ar^+ ions dramatically change the growth mode in Ag/Ag(111), from multilayer (3D) to 2D growth. The island

number density in homoepitiaxial growth in Pt(111) is also shown to change in the presence of an Ar^+ beam in the 0.4–4 keV ion energetic range.[21] A second line of application is in connection with the generation by high-dose irradiation of surfaces with periodic ripple or dot structures,[22] which are thought to respond to fundamental scaling laws.[23] Apart from its intrinsic technical interest, these experiments have proved to be very valuable to gain knowledge about atomic parameters involved in diffusion processes, for example, Schwoebel barriers. The importance of better knowing the thermodynamics and kinetics of surface defects in order to control these technological processes is hard to overemphasize.

In this paper, we carry out an analysis of the different defect structures produced at 300 K by bombardment of the reconstructed Au(001) surface with 600 eV Ar^+ ions. Also some preliminary results for Pt(001) are reported. We present a comparative STM analysis of the whole range of doses between approximately 10^{13} and 10^{16} ions/cm^2, with emphasis on the initial low-dose stages. The role of higher sample temperatures and lower ion fluxes is also investigated. Molecular dynamics simulations are performed in parallel to compare ideal defect structures with the experimental images and to gain insight into the dynamics of defect evolution, from the primary damage (i.e., mainly vacancies) to more complex structures. At doses comparatively lower than in previous studies, a new type of defect is found that is characterized as a 2D dislocation dipole. These dipoles, and the dislocations resulting from their dissociation, are shown to represent one of the few examples of dislocation structures in quasi-2D systems. For higher doses the transit from dislocation dipoles to vacancy islands is also characterized. At the higher edge of the dose range, surface morphologies involving multiple-level square pits, similar to the ones observed in other fcc metals,[24,25] are observed, and their evolution from the medium-dose damage identified and explained in terms of a simple model.

II. EXPERIMENT

The experiments were performed in an ultrahigh-vacuum chamber equipped with Auger electron spectroscopy (AES), low-energy electron diffraction (LEED), and a homemade STM based on an earlier published design.[26] The chamber was pumped by an ion pump, a titanium sublimation pump, and a turbomolecular pump. The base pressure of the chamber was in the range of 10^{-10} mbar. The clean Au(001) sample, monitored by AES, was prepared by cycles of 600 eV Ar^+ bombardment and subsequent high-temperature annealing. As checked by STM and LEED, the clean surface exhibits atomically flat terraces with an average width of about 100 nm and the well-known[27] $5\times n(n\simeq 25)$ reconstruction. This reconstructed surface has an a real atom density about 17% larger than that of the unreconstructed Au(001).

Defects were created by 600 eV Ar^+ bombardment, using a differentially pumped ion gun. To ensure a homogeneous dose over the area probed by the STM, the ion beam was swept over a 3×3 mm^2 area of the sample, the integral ion dose being directly monitored with a Faraday cage. Typical fluxes Φ were of the order of 10^{12} $Ar^+cm^{-2}s^{-1}$. Irradiations were performed by exposing the sample to the beam for a certain time keeping the crystal at 300 K. The doses are reported in units of the atomic surface density of the *unreconstructed* Au(001) surface, which is of 1.21×10^{15} cm^{-2}. Thus, one ion per surface atom will be referred to as 1 ML$^+$ or *one equivalent ion monolayer*. To analyze the interaction of adatoms with bombardment-induced damage a number of runs were conducted in which Au was evaporated onto the previously damaged sample from a tungsten filament under ultrahigh-vacuum conditions.

STM images were obtained at 300 K in the constant-current mode. Typically, the tunnel current was 0.1 nA, with a tunneling voltage of 50–500 mV applied to a tungsten tip. By comparing successive images of the same area it was found that voltages above 1 V accelerated the kinetics of surface evolution. Below that voltage, we did not recognize any tip effects, but one cannot discard the idea that some of the surface evolution discussed below, as detected in images of the same area after a time lapse of several minutes, could actually have been accelerated by the electric field under the tip. As a working recipe, on the basis of our own experience, we tried to keep the bias voltage as low as possible.

III. SIMULATION DETAILS

Molecular dynamics simulations have been performed to provide theoretical support to our experimental observations. We have used the many-body glue potential to simulate the interatomic forces in Au. The glue model[28] has proven to be reliable for Au since its reconstructed low-index surfaces appear as energetically favorable. For example, for Au(001) the 5×34 structure results to be the one with the lowest energy, very close to the 5×25 reconstruction revealed by STM.

The model system consists of a slab with lateral periodic boundary conditions its size depending on the specific simulation. It varies between 8 and 15 layers in the surface normal direction, 3–10 periods in the short-reconstruction direction (15–50 atomic distances), and 1–3 periods in the long-reconstruction direction (34–102 atomic distances). We work on the basis of a 5×34 reconstruction as this is the optimal periodicity resulting from the glue potential. The total number of atoms is between 10 000 and 50 000. Newtonian equations are integrated using the Verlet algorithm with a time step between 2 and 5 fs. The temperature is fixed at the desired value by rescaling atomic velocities at each time step, whereas pressure is always kept to zero by modifying the cell lateral dimensions. To analyze the structure, we always relax the system to its local minimum in order to eliminate the vibrational noise. This is done by using a conjugate gradient algorithm that minimizes the potential energy.

IV. RESULTS AND DISCUSSION

A. Irradiated surfaces: Low doses (<0.05 ML$^+$)

Figure 1 shows a STM image of the clean Au(001) surface, prior to the ion bombardment. A similar STM image is obtained for the clean Pt(001) reconstructed surface. The

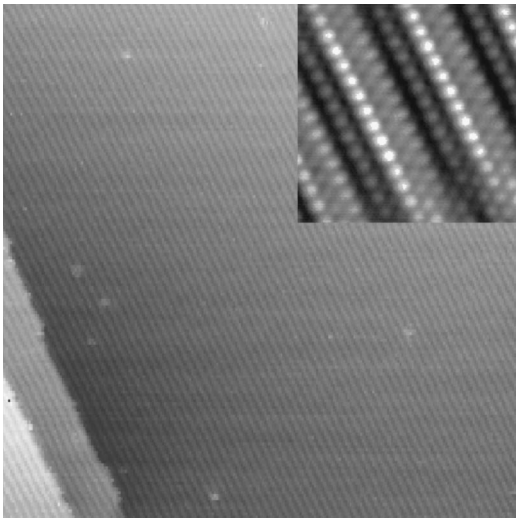

FIG. 1. Clean hexagonal-reconstructed Au(001) STM image showing a typical broad terrace with two monatomic steps on the left (100×100 nm^2). Inset: An atomic resolution image of the same area (3.7×3.7 nm^2).

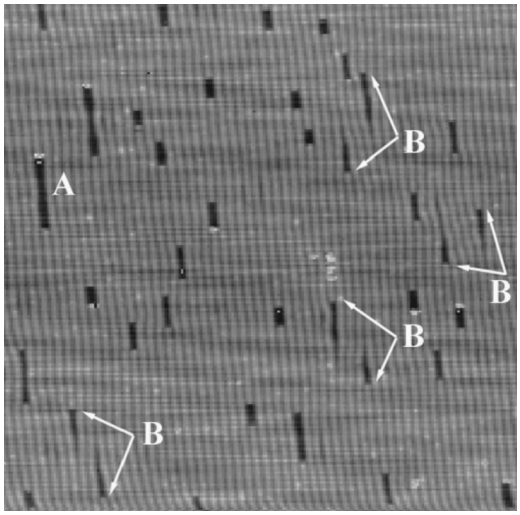

FIG. 2. The Au(001) surface after bombardment with 0.05 ML$^+$ of 600 eV Ar$^+$ at 300 K. (83×83 nm^2). (A) Depressions and (B) individual dislocations (always in pairs with $\theta \neq \pi/3$).

fringes are due to the short periodicity (1.44 nm) of the so-called $5\times n$ ($n\simeq25$) reconstruction.[27] Clean surfaces typically consist of terraces 100 nm wide, separated by steps of monatomic height (0.20 nm). Reconstruction fringes run along the $\langle 110\rangle$ step directions of the substrate, and, nearly in all terraces, only one of the two possible orientations is observed, that direction being in general parallel to the steps encompassing the terrace. In the many images of clean surfaces that have been analyzed, no defects (vacancy or adatom islands, dislocations) other than steps are apparent. Sometimes (see Fig. 1), some bright spots are visible, which might correspond to impurities below the Auger detection limit. Whatever the subsequent treatments of the sample (e.g., bombardments), this clean-surface topography is recovered after annealing for a few minutes at about 900–950 K.

1. Dislocations and dislocation dipoles

Figure 2 shows the reconstructed Au(001) surface after bombardment with 600 eV Ar$^+$ ions at 300 K. The dose is 0.05 ML$^+$. As can be seen in this image, there are no traces of vacancy or adatom islands. The only visible defects are (i) elongated rectangular depressions (labeled A in the figure), 0.06 ± 0.01 nm deep and one short period of the reconstruction wide and (ii) *forklike* features (B), in which a reconstruction line appears to bifurcate from a given point. As discussed in an earlier publication,[29] depressions cannot be interpreted as vacancy islands but as two-dimensional (2D) dislocation dipoles of opposite Burgers vectors. Similarly, forklike features labeled B in Fig. 2 are the Moiré-enhanced footprints of individual dislocations. The line joining the two opposite dislocations forms an angle of $\theta=\pi/3$ with the direction defining the Burgers vectors: this type of dipole is commonly named a $\pi/3$ dipole.[30] The individual 2D dislocations are seen to appear generally in pairs and thought to originate from the dissociation of 2D dislocation depressions.[31]

Strong experimental support to this interpretation comes from the observation of typical dislocation behavior of both depressions and forklike structures, a flavor of which can be derived from the various examples summarized in Fig. 3. In this figure, STM images of the same area are shown after time lapses of the order of an hour at room temperature, often under long periods of STM observation. Figure 3(a) shows the formation of a depression after one of the two components of a pair of interacting dislocations (initially at $\theta\neq\pi/3$) glides into the other. Figure 3(a) also shows a reaction involving originally two depressions. Each of these depressions dissociates into a pair of opposite dislocations. Two of these dislocations glide onto each other on the same plane and eventually annihilate, leaving behind the two surviving dislocations, which glide apart. Some depressions (as the one initially marked C) also disappear, probably due to adatom incorporation to their cores. Figure 3(b) shows gliding of a single dislocation along the compact direction of the hexagonal overlayer. Finally, in Fig. 3(c) we present images of two depressions that have glided while preserving their identity. In the next subsection we shall explain how these and other examples can be understood in terms of a simple dislocation model.

STM images taken at room temperature of surfaces bombarded at 400 K reveal a greater proportion of individual dislocations with respect to depressions than after room temperature bombardment. The same effect is observed when a sample bombarded at room temperature is annealed at 400 K and then imaged at 300 K. It can be concluded that depressions tend to be unstable at high temperatures. Occasionally, dislocations align themselves, forming a 2D low-angle grain boundary that separates two reconstruction domains of different orientation (Fig. 4). This provides more evidence that dislocation glide processes are operative in this system.

To gain further insight into the nature of depressions, we studied their evolution in the presence of an excess of adatoms. When less than 0.1 ML of Au is evaporated on top of

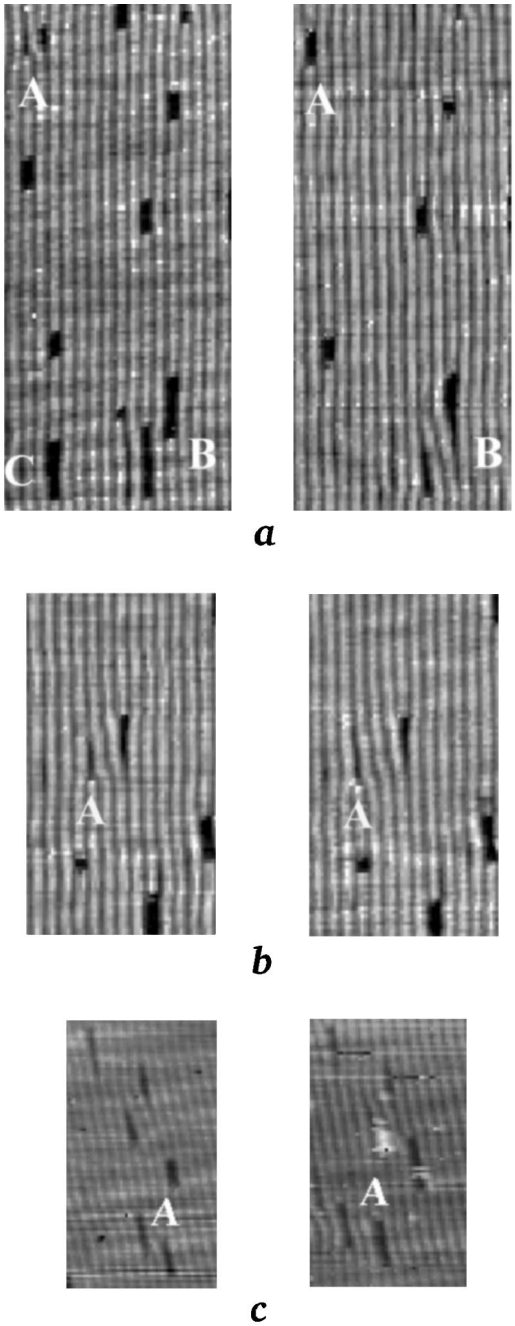

FIG. 3. Examples of dislocation behavior of the defects of Fig. 2. The same areas are imaged after times of the order of an hour. (a) On top of A: a dislocation glides into another resulting in a depression; on the left of B: two depressions dissociating and giving rise to two dislocations; on the right of C: depression disappearing. (b) Gliding of a single dislocation on top of A. (c) Two depressions below A glide two and three reconstruction periods, respectively.

an irradiated sample, adatom islands 0.2 nm high appear, while depressions are seen to vanish. The mechanism involved in the latter process is most likely dislocation climbing (depression shrinkage) through adatom incorporation, leading to dislocation annihilation when both cores meet.

Along with the systematic study described above for Au(001) a number of similar irradiation and STM runs were performed on a Pt(001) surface.[32] From a morphological point of view, the damage looks very similar in both metals: depressions and single dislocations are observed.

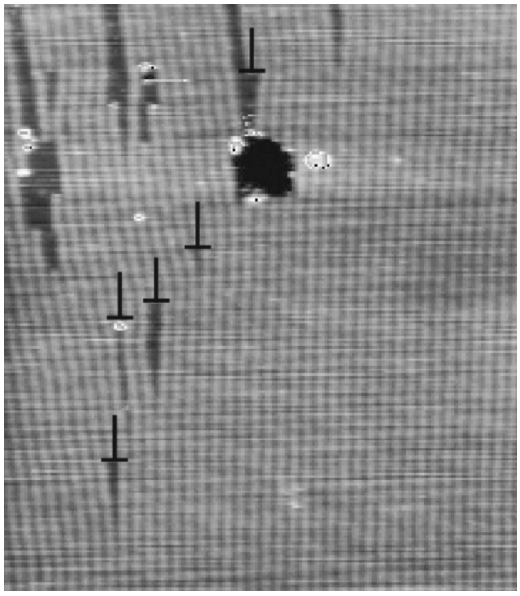

FIG. 4. Dislocations aligned in a 2D low-angle grain boundary as shown by STM in a sample that has been bombarded and annealed (64×64 nm^2). Note the different reconstruction orientations on the right and left sides of the dislocation boundary.

2. Two-dimensional dislocations in reconstructed layers

Observations as the ones discussed above leave little doubt that the defects involved behave like 2D dislocations. Indeed 2D dislocations have been the subject of much theoretical work[33] and our results suggest that the Au(001) topmost reconstructed layer, whose theoretical defect characteristics have begun to be elucidated,[34] may well serve as a playground for the verification of some of their predictions.

Let us consider a 2D dislocation pair with opposite Burgers vectors $\pm\vec{b}$. Let x and y be the distance between the two dislocations, respectively, along their common gliding direction and its normal, both in units of next-neighbor distance. If θ is the angle between that gliding line and the line joining the dislocations, we can write the interaction energy per unit length U_{int} as

$$U_{int}=2\epsilon_c b^2+Jb^2\left(\ln\frac{y}{r_c\sin\theta}-\frac{1}{2}\cos 2\theta\right)+A\cos\left(\frac{2\pi x}{6}\right), \tag{1}$$

where ϵ_c and r_c refer, respectively, to the energy per unit the volume and radius of the dislocation core and J can be written in terms of the Lamé and Poisson moduli μ and ν as $J=\mu(1-\nu)/2\pi$. The first two terms express the well-known interaction energy in terms of isotropic elasticity,[30] whereas we have added a third term, scaled by an amplitude A, which takes into account the difference in energy when the dipole sits on the ridge of the corrugation and at the bottom of the valley.

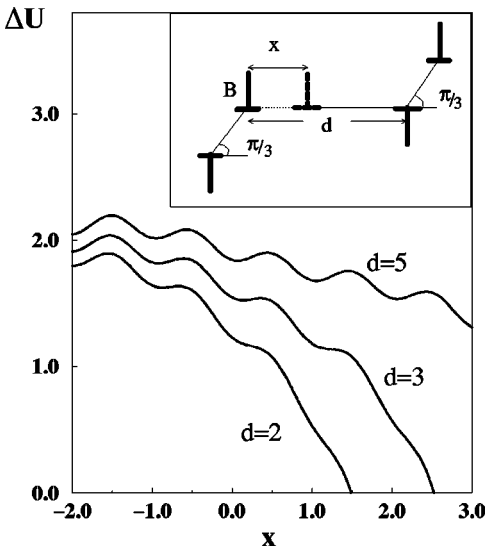

FIG. 5. Interaction energy of the four dislocations configuration shown in the inset, on the basis of Eq. (1) as a function of the position x of the dislocation B ($x=0$ corresponds to a $\pi/3$ dipole). The distance d between the two depressions corresponds to an integer number of corrugation periods.

For sufficiently high values of A, the inclusion of the last term in Eq. (1) results in a series of metastable minima in the U_{int} vs x plot (equivalent to a plot of U_{int} vs θ), which correspond to the successive on-ridge positions of the dipole. One of these minima, with $\theta=\pi/3$, accounts for the observed geometry of depressions.[35]

There can be at least two driving forces for the dissociation of a depression: one is temperature, as the entropy contribution might dominate the free energy resulting in a dissociated state. The other arises from the presence of external elastic forces acting on the depression. The configuration corresponding to Fig. 3(a)(B) is an example of the latter, in which a second nearby depression acts as a dissociating agent. In Fig. 5 we plot the elastic energy of the configuration of two depressions, whose details and parameters are shown in the inset. It is easy to see that the presence of the second depression reduces the dissociation barrier of the first, this barrier even vanishing for a sufficiently short distance between the depressions. These results can be used to explain the reaction observed in Fig. 3(a)(B).

Due to the different symmetry between the topmost reconstructed layer and the substrate, this interface can be described in terms of a grain boundary between a 3D and a 2D crystal, where 2D dislocations can end up. These 2D dislocations should not be confused with the several systems of misfit dislocations that have been extensively described in the literature of multilayer growth[36,37] and that are sometimes called *surface dislocations*. For example, in reconstructed surfaces such as Au(111) or Pt(111,)[37,38] the frontier between a fcc and a hcp region is a Shockley partial dislocation, which runs parallel to the surface. At the point where two of these Shockley partial dislocations meet, a perfect edge dislocation (threading dislocation) is formed that runs from the second layer to the surface. Both partial and threading dislocations reside in the first and second layers at a variance with dislocations and depressions in reconstructed Au(001), which are constrained solely to the top layer. The latter end up at the boundary between this reconstructed layer and the crystal bulk, due to their different symmetry (hexagonal and square, respectively). In contrast to 3D dislocations, which are line defects, 2D dislocations are pointlike.

The defects described in the present paper are an experimental realization of those 2D dislocations, which have received much theoretical attention, particularly in connection with order-disorder 2D transitions.[39] We argue that reconstruction plays a fundamental role in the creation of these 2D dislocation structures, since they are not observed in unreconstructed metal surfaces subjected to similar radiation conditions (ion mass, energy, temperature, etc.). This might be understood in terms of the so-called floating nature of the reconstructed overlayer.[40]

3. The origin of two-dimensional dislocations: Molecular dynamics simulations

Radiation damage in the *bulk* of solids is well characterized. Currently,[41] *knock-on* defects of maximum energy 340 eV are produced in Au by impinging 600 eV Ar^+ ions and no more than a few point defects per ion are expected to result. Furthermore, these defects are known to be generated very near to the surface. In spite of recent advances,[42,43] the understanding of damage evolution near a surface is still subject to much uncertainty, for example, concerning the role of thermal spikes. Experiments in recent years have shown that the observed surface damage consists of surface vacancy islands,[12–16] and, under certain conditions of flux and temperature,[13] of adatom islands. Also, at energies below 1 keV, the total adatom and vacancy yield per incoming ion has been shown to be close to unity.[14] Consequently, surface defect diffusion must play a substantial role in the configuration of the observed damage.

On that basis, we proposed earlier[10] that the observed depressions (or, eventually, dislocations) originate from the clustering and further collapse of surface vacancies. We discuss now how molecular dynamics simulations[44] using the glue potential[28] support this view. We start with a Au(001) reconstructed surface plus a set of randomly distributed vacancies to model the vacancies created by ion impacts. These are simulated by eliminating an atom from the overlayer and letting the simulation evolve in time. The results of the simulation show that surface vacancies migrate to the reconstruction ridges and diffuse anisotropically along them (see Fig. 6). In fact, anisotropic diffusion has been shown earlier for adatoms in Au (001) and Pt(001).[45]

This process ends up in vacancy rows along the ridges, a result that can be understood in physical terms since vacancies are actually expected to have lower energy when placed on the reconstruction ridges (on top, less coordinated sites). These rows are the nuclei of depressions since we have shown in an earlier work[10] that vacancy rows in a reconstruction ridge collapse into dislocation dipoles. Furthermore, molecular dynamics simulations can account for other experimentally observed processes, such as the depression dissociation of Fig. 3. Simulations carried out at 975 K show

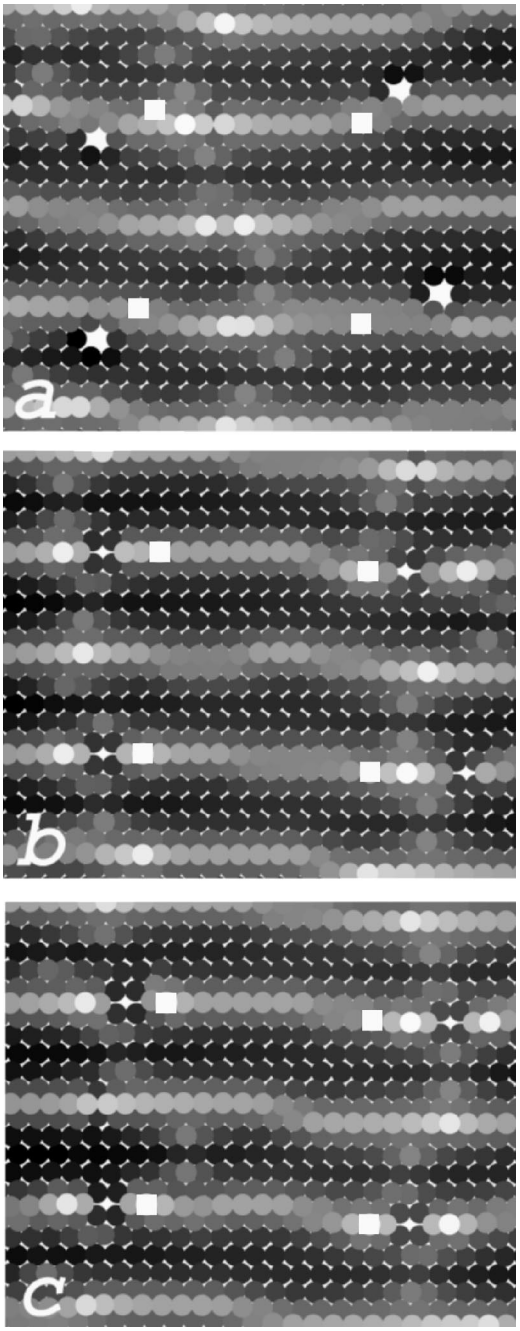

FIG. 6. Molecular dynamics simulation of vacancy transport on a hexagonal-reconstructed Au(001) surface. Four vacancies (a) initially placed at random on the corrugated surface, (b) are seen to climb into the corrugation ridge, and (c) anisotropically diffuse along the latter. The white squares are a fixed reference.

that, in times of a few ns, a depression evolves into a configuration of two opposite individual dislocations on contiguous corrugation valleys. To explore alternative atomic configurations in a depression, the stability of an unreconstructed region (local square symmetry), one reconstruction period wide, was investigated. Molecular dynamics simulations showed that this structure becomes unstable and atoms arrange in a 2D dislocation dipole configuration (depression).

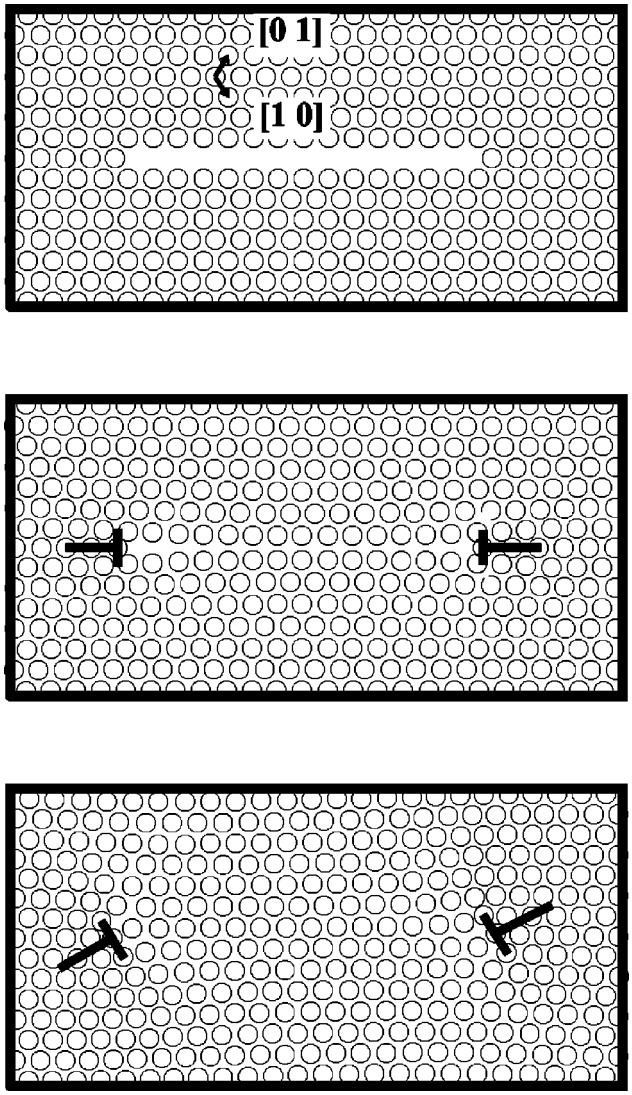

FIG. 7. Sketch of the atom positions, according to elasticity equations, for the following 2D defects: (a) a row of vacancies along $[11]$; (b) a Frank dislocation dipole with $\pm\vec{b}=(a/2)[1\bar{1}]$; (c) a perfect dislocation dipole (depression) with $\pm\vec{b}=a[10]$.

The collapse of a *row* of vacancies is the 2D equivalent of the 3D collapse of a *disk* of vacancies. With reference to Fig. 7, in which the directions in the topmost reconstructed layer are expressed in terms of only two coordinates, a vacancy row (a) along the $[11]$ direction collapses into a 2D stacking-fault (b) encompassed by two 2-D dislocations at both ends. Assuming that Burgers circuits are taken counterclockwise, the Burgers vectors of both dislocations will be $(a/2)[1\bar{1}]$ and $(a/2)[\bar{1}1]$, where a is the interatomic distance. From the point of view of their geometries and strain fields, these dislocations are 2D partial dislocations of Frank type, i.e., the two-dimensional analog of the well-known dislocation loops that originate from the collapse of a vacancy disk in the bulk. They can be thought of as the intersection with the surface of 3D dislocation loops with a well-defined Burgers vector. The diameter of the 3D loop is then equivalent to the length of the 2D dipole.

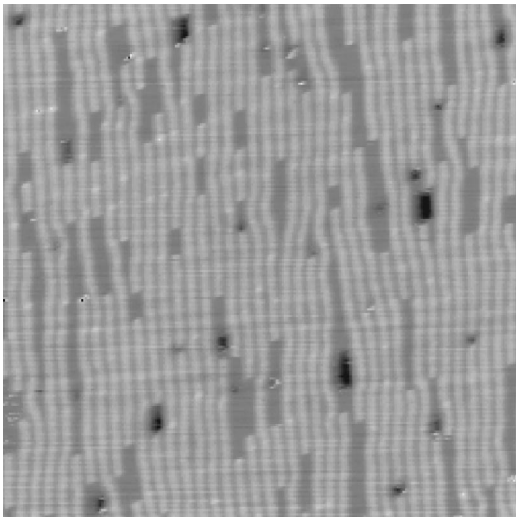

FIG. 8. STM image of an Au(001) surface after being irradiated with a dose of 0.1 ML^+ (60×60 nm^2). Vacancy islands (darker in the image) are now conspicuous. Note that nucleation of vacancy islands of 0.2 nm depth takes place on existing dislocation dipoles.

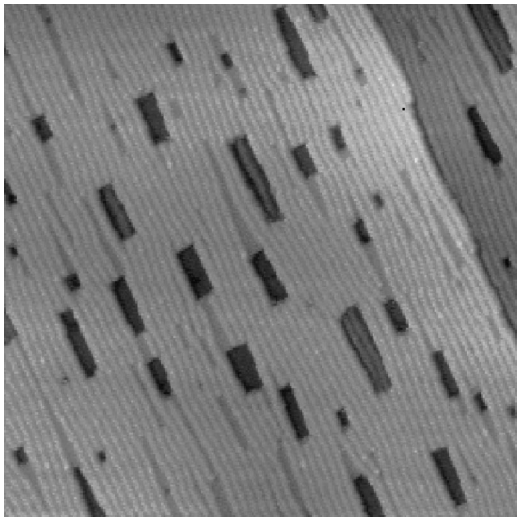

FIG. 9. STM image of an Au(001) surface after being irradiated with a dose of 0.25 ML^+ (89×89 nm^2). Large vacancy islands are present, together with elongated troughs, the latter 0.06 nm deep.

In Fig. 7(c) the above 2D Frank-like dislocations unfault by nucleating 2D Shockley-like dislocations of, respectively, Burgers vectors $(a/2)[11]$ and $(a/2)[\bar{1}\bar{1}]$. The dislocation reactions involved are then[46]

$$\frac{a}{2}[1\bar{1}]+\frac{a}{2}[11]=a[10], \tag{2a}$$

$$\frac{a}{2}[\bar{1}1]+\frac{a}{2}[\bar{1}\bar{1}]=a[\bar{1}0], \tag{2b}$$

which lead to a final state consisting of a pair of perfect dislocations whose Burgers vectors are along [10]. Obviously, the nucleation of the opposite Shockley dislocations would have led also to a pair of perfect dislocations with Burgers vectors along the other compact direction, respectively, $[0\bar{1}]$ and [01]. Note that a Frank-like dipole [such as that of Fig. 7(b)] can be, alternatively, described as an unreconstructed area one atom wide. However, only the description in terms of a dipole of perfect dislocations [Fig. 7(c)] can explain the physical processes taking place after the reaction of Eq. (2) occurs.

B. Medium doses (0.1 ML^+–0.3 ML^+)

An image of a reconstructed Au(001) surface bombarded at a dose of $\simeq 0.1$ ML^+ is shown in Fig. 8. New features are seen, apart from the dislocation dipoles and individual dislocations observed at lower doses. Several vacancy islands 0.2 nm deep (in contrast to the 0.06 nm depth of depressions) appear in the image. The transition from an only-dislocation stage to a vacancy islands and dislocations stage is characterized by the following property: vacancy islands always nucleate either at the center or near the corner of dislocation dipoles, as can be seen in Fig. 8. A tentative explanation follows: ions impinging over nondefective sites of the surface yield vacancies that evolve as discussed above, resulting in dipole growth by climbing or, eventually, originating new dislocation dipoles. On the other hand, when an ion impinges on a dipole, the new vacancies are confined into the core region of the dipole and a vacancy island may be nucleated. Thus, a low-vacancy density would arrange itself in dislocation dipoles, whereas a higher vacancy density would condense into vacancy islands. According to these ideas, the nucleation of a vacancy island would take place after a certain vacancy density was reached.

For still higher doses, ~ 0.2–0.3 ML^+, larger vacancy islands become abundant, as can be seen in Fig. 9. Note the presence of *troughs*, protruding from some vacancy islands, with a depth of 0.06 ± 0.01 nm. They also have a dislocation

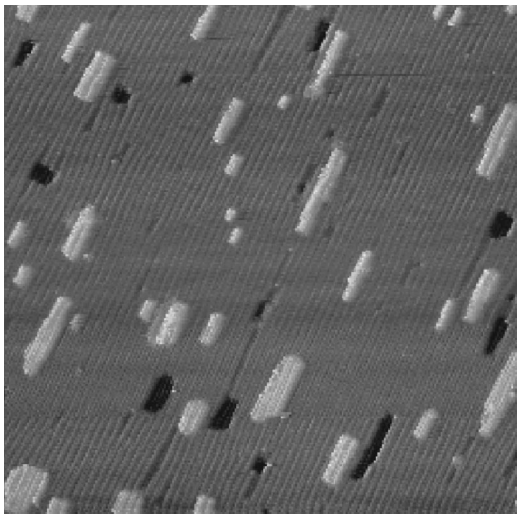

FIG. 10. Clean hexagonal-reconstructed Au(001) surface after evaporation of slightly more than 1 ML of Au (unbombarded surface) (105×105 nm^2). Adatom and vacancy islands, elongated troughs, dislocations, and depressions are visible.

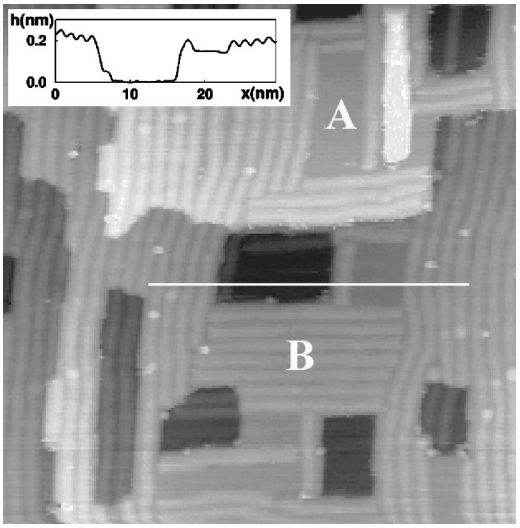

FIG. 11. (a) STM image of an Au(001) surface after being irradiated at 300 K with a dose of 0.5 ML^+ (42×42 nm^2). In addition to vacancy islands one observes (A) unreconstructed patches and (B) perpendicular-reconstruction domains. Inset: depth profile of two contiguous unreconstructed patches, one of them inside a vacancy island.

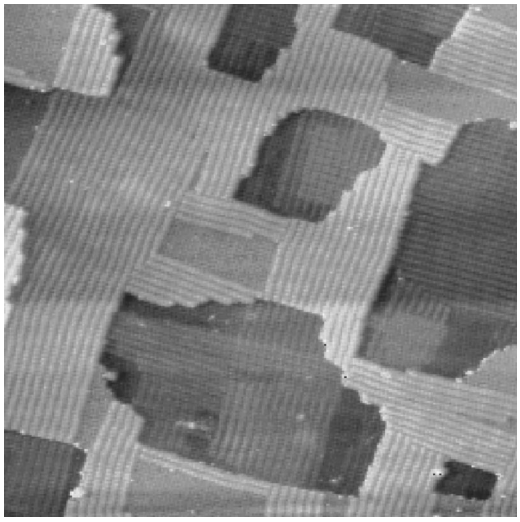

FIG. 12. Pt(001) bombarded and mildly annealed (89×89 nm^2). Note the similarities of the defects with those in Fig. 14 for an Au(001) surface.

character, being the remnants of long depressions that have nucleated a vacancy island on one of its ends and later become dissociated.

A further check of the model is provided by an experiment, in which Au is evaporated onto a clean *unbombarded* reconstructed surface. Evaporating slightly more than 1 ML Au yields surface images like that shown in Fig. 10. The topographic image looks very similar to Fig. 9, taken after medium-dose ion bombardment. This similarity is remarkable. We offer the following explanation: at very low coverages, adatom islands 1.44 nm wide nucleate on top of nonequivalent substrate sites. With increasing coverages, the islands grow laterally, propagating the reconstruction fringes. For coverages close to 1 ML, the reconstruction fringes do not match exactly, and the mismatch is accounted by relaxed vacancy rows, that is, depressions or 2D dislocation dipoles, some of which can be very long.

C. High doses (>0.5 ML^+)

A STM image of a sample after ion bombardment at a dose of $\simeq0.5$ ML^+ is shown in Fig. 11. In addition to large, reconstructed vacancy islands, a new type of feature is observed, exemplified by A in that figure. These features are deconstructed patches with well-defined straight sides, parallel to the compact directions of the substrate. Their mean depth (measured with respect to the mean value of the corrugation of the reconstructed layer) is 0.06 ± 0.01 nm, which agrees well with the profile of a hard-sphere model. Furthermore, higher-resolution STM reveals that atoms in deconstructed areas indeed exhibit square symmetry. Note that these deconstructed patches are always encompassed by perpendicular reconstruction domains, in contrast to the as-prepared surface in which only a single domain is present in any given terrace. We shall name this phenomenon *deconstruction*, resulting in *deconstructed areas*.

The defects and features described in Au are also observed in Pt(001) when bombarded in the same range of doses as shown in Fig. 12. One should also remark that deconstructed areas are visible with the same symmetry than those of Au although they seem to be more ubiquitous for comparable doses. The 5×5 reconstruction distinctive of Pt also appears,[47] this reconstruction being usually present when two perpendicular domains cross each other.

The origin of this deconstruction is not clear. As is well known the 5×1 reconstruction of Pt(001) can be lifted by CO adsorption,[48] and it could be argued that some kind of contamination might be responsible for deconstruction in bombarded Au(001). There are several facts that rule out this possibility. First we recall the almost negligible sticking coefficient for reactive gases of Au, as compared to that of Pt. Also, we point out that no traces of adatom or molecule clusters are visible on the surface. We have shown above that gold adatoms are captured by dislocation dipoles, and that, only when in excess, subsequently cluster to give rise to islands. Previous observations have shown that were there any contaminant molecules on the surface, they would show up as bumps on the surface, very likely with a height different from 0.2 nm. Moreover, previous investigations[47] of CO adsorbed onto Pt(001) show unreconstructed patches of adsorbed CO that bear no relation to the well-defined rectangular shapes of our deconstructed areas. In the absence of contamination effects, we suggest that the patches of deconstruction are linked to reconstruction instabilities, the latter triggered by an increase of the local density of surface atoms in the patch. Further evidence for this interpretation is provided in the next subsection.

To help elucidating the influence of temperature in the final morphology of the surface, some ion bombardment experiments have been performed with the sample at higher temperature ($\simeq400$ K). While the ion dose is comparable with that of Fig. 11, the topography is clearly different. The

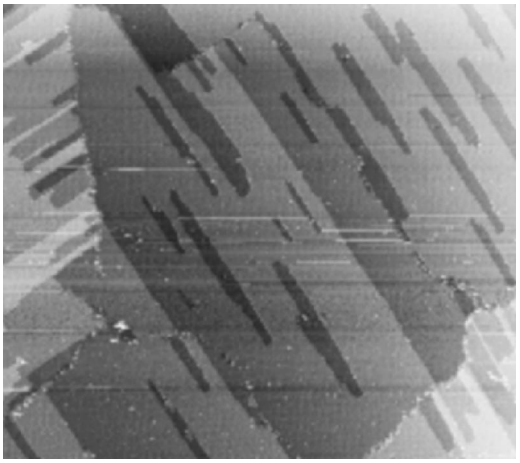

FIG. 13. Surface bombarded with a dose of 0.5 ML^+, comparable to that of Fig. 14, but with the surface at 400 K (500×400 nm^2).

image shown as Fig. 13, encompassing a wide area, reveals very large vacancy islands, whereas unreconstructed regions or perpendicular reconstruction domains are not visible. Note the elongated shape along the reconstruction direction of the large vacancy islands. In some cases, vacancy island growth competes with step retraction. In addition, a very small amount of dislocations are present. These observations are in good agreement with a model of diffusion-controlled vacancy accretion by growing vacancy islands. In fact, any rate equations in terms of competition between island growth and annealing at sinks (steps and the like) yield the same general result: high temperature and/or low ion flux lead to a few large vacancy islands, whereas a high concentration of vacancy islands is expected for the opposite conditions.

D. Very high doses ($\gg 1$ ML^+)

Extending the ion bombardment to these very high doses results in coalescence of the vacancy islands, which become irregularly shaped, and formation of a multilevel structure, whereas no perpendicular reconstruction domains are visible. The morphology of the damage can be also easily explained in terms of vacancy diffusion kinetics. The final number of exposed levels depends basically on the probability of nucleating a new vacancy island inside a previous one. Deep vacancy pits imply that new vacancies have been able to nucleate and give rise to an island before they annihilate with vacancy steps. For a given temperature this is possible only if the rate of vacancy creation, i.e., the flux, is high enough.

We have performed a number of irradiations with a flux five times higher than the usual one. Compared with the experiments at lower fluxes, the resulting damaged surface shows, on the average, more vacancy pits of smaller area and with more multiple levels. As an example, Fig. 14 shows that this high-flux irradiation with a dose of about 10 ML^+ results in pits with square symmetry, several atomic layers deep. Their morphology is entirely similar to earlier-described results on (001) and (111) nonreconstructed fcc surfaces.[25,49] Under STM conditions, significant evolution takes place in times of the order of hundreds of minutes at

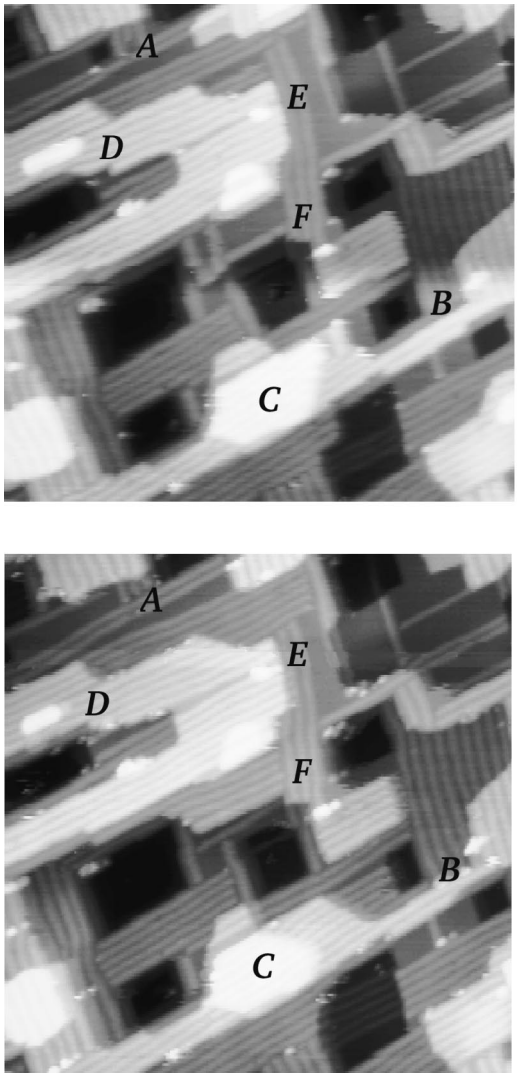

FIG. 14. Several annealing processes are clearly visible in this two images of a highly bombarded surface (10 ML^+) with a time interval of one hour between them (from top to bottom) (56×56 nm^2). The most interesting are (i) a vacancy island disappears on the left of A, while another one shrinks on the left of B; (ii) two adatom islands shrink in C and on the left of D; (iii) the reconstruction grows over E and at a previously unreconstructed patch on the left of F.

room temperature; as examples see in Fig. 14 (i) the disappearance of the deepest level at a multi-level vacancy pit; (ii) vacancy crater shrinkage; (iii) transfer of vacancies between two contiguous levels; and (iv) adatom island shrinkage. A most revealing process linked to the evolution of deconstructed areas is also visible in the figure: the deconstructed area at F is seen to reconstruct. We take it as a strong suggestion that an increase in the local density of surface atoms reverts the deconstruction.

The existence of multiple-level vacancy pits as those discussed above might be taken, at first sight, as evidence of the existence of Schwoebel barriers. However, Constantini *et al.*[24] in nonreconstructed Ag(001) have shown that this is not an essential requirement and that a suitable interplay between temperature, flux, and dose can result in a full range of

morphologies. Our results in reconstructed Au(001) are very similar to theirs and suggest that, after very high doses, reconstruction does not play a substantial role in the resulting damage.

V. CONCLUSIONS

The main conclusion of this work is that ion irradiation at low doses of reconstructed Au(001) surfaces results in the creation of dislocations and dislocation dipoles on the topmost hexagonal layer and that this layer behaves as a 2D dislocation system. Furthermore, these 2D dislocations are seen to react, glide, climb, etc., in much the same way as bulk dislocations do. They appear frequently in the form of dipoles at an angle of $\theta = \pi/3$, which after higher doses become the nucleation centers of the vacancy islands commonly observed by other researchers in a variety of metal surfaces. Defects with the same morphology appear under comparable bombardment doses in reconstructed Pt(001).

Molecular dynamics simulations show that the origin of these dislocation structures can be understood in terms of anisotropic diffusion processes involving bombardment-induced vacancies. At higher doses, in the neighborhood of one ion per surface atom, apart from vacancy islands new types of defects are recognized, one of which is characterized as deconstructed patches of (001) symmetry. These patches are likely to develop from reconstruction instabilities induced by an excess of vacancies in regions in which competing reconstruction orientations can lead to reconstruction frustration. The observation of processes in which a deconstructed patch reconstructs supports this explanation.

ACKNOWLEDGMENTS

This research has been supported by a grant from the Spanish DGICYT Contract No. PB96-0652, which is gratefully acknowledged. O.R.F. wants to thank the Spanish Ministry of Education and Culture for a financial support. We thank Dr. J.M. Soler for his help in implementing the computational code for the glue potential.

*Corresponding author, FAX: +34 91 394 45 47. Email: oscar@material.fis.ucm.es

[1] D.B. Williams and C. Barry Carter, *Transmission Electron Microscopy* (Plenum Press, New York, 1996).

[2] G. Somorjai, *Surface Chemistry and Catalysis* (Wiley, New York, 1996).

[3] G. Boisvert and L.J. Lewis, Phys. Rev. B **54**, 2880 (1996); G. Boisvert, L.J. Lewis, M.J. Puska, and R.M. Nieminen, *ibid.* **56**, 7643 (1997).

[4] J.B. Hannon, C. Klünker, M. Giesen, H. Ibach, N.C. Bartelt, and J.C. Hamilton, Phys. Rev. Lett. **79**, 2506 (1990).

[5] A. Samsavar, E.S. Hirschorn, T. Miller, F.M. Leibsle, J.A. Eades, and T.-C. Chiang, Phys. Rev. Lett. **65**, 1607 (1990).

[6] M. Schmid, A. Biedermann, H. Stadler, and P. Varga, Phys. Rev. Lett. **69**, 925 (1992).

[7] J. Jacobsen, L. Pleth Nielsen, F. Besenbacher, I. Stensgaard, E. Lægsgaard, T. Rasmussen, K.W. Jacobsen, and J.K. Nørskov, Phys. Rev. Lett. **75**, 489 (1995).

[8] A.K. Schmid, N.C. Bartelt, J.C. Hamilton, C.B. Carter, and R.Q. Hwang, Phys. Rev. Lett. **78**, 3507 (1997).

[9] J. de la Figuera, M.A. González, R. García-Martínez, J.M. Rojo, O.S. Hernán, A.L. Vázquez de Parga, and R. Miranda, Phys. Rev. B **58**, 1169 (1998).

[10] M.A. González, J. de la Figuera, O. Rodríguez de la Fuente, and J.M. Rojo, Surf. Sci. **429**, L486 (1999).

[11] Zheng Gai, Yi He, Xiaowei Li, J.F. Jia, and W.S. Yang, Surf. Sci. **365**, 96 (1996).

[12] C.A. Lang, C.F. Quate, and J. Nogami, Phys. Rev. Lett. **59**, 1696 (1991).

[13] T. Michely and G. Comsa, Phys. Rev. B **44**, 8411 (1991).

[14] T. Michely and Ch. Teichert, Phys. Rev. B **50**, 11 156 (1994).

[15] J.C. Girard, Y. Samson, S. Gauthier, S. Rousset, and J. Klein, Surf. Sci. **302**, 73 (1994).

[16] S. Gauthier, Y. Samson, J.C. Girard, S. Rousset, and J. Klein, J. Vac. Sci. Technol. B **12**, 1754 (1994).

[17] M. Ghaly, R.S. Averback, and T. Díaz de la Rubia, Nucl. Instrum. Methods Phys. Res. B **102**, 51 (1995).

[18] W. Sindo and T. Ohmi, J. Appl. Phys. **79**, 2347 (1996); P.C. McIntyre, K.G. Ressler, N. Sonnenberg, and M.J. Cima, J. Vac. Sci. Technol. A **14**, 210 (1996).

[19] R. Ditchfield and E.G. Seebauer, Phys. Rev. Lett. **82**, 1185 (1999).

[20] G. Rosenfeld, R. Servaty, Ch. Teichert, B. Poelsema, and G. Comsa, Phys. Rev. Lett. **71**, 895 (1993).

[21] S. Esch, M. Breeman, M. Morgenstern, T. Michely, and G. Comsa, Surf. Sci. **365**, 187 (1996).

[22] S. Rusponi, G. Constantini, C. Boragno, and U. Valbusa, Phys. Rev. Lett. **81**, 2735 (1998); **81**, 4184 (1998); M.V. Ramana Murty *et al. ibid.* **80**, 4713 (1998); S. Facsko, T. Dekorsy, C. Koerdt, C. Trappe, H. Kurz, A. Vogt, and H.L. Hartnagel, Science **285**, 1551 (1999).

[23] M. Kardar, G. Parisi, and Y-C. Zhang, Phys. Rev. Lett. **56**, 889 (1986).

[24] G. Constantini, S. Rusponi, R. Gianotti, C. Boragno, and U. Valbusa, Surf. Sci. **416**, 245 (1998).

[25] M. Ritter, M. Stindtmann, M. Farle, and K. Baberschke, Surf. Sci. **348**, 243 (1996).

[26] D.M. Zeglinski, D.F. Ogletree, T.P.J. Beebe, R.Q. Hwang, G.A. Somorjai, and M.B. Salmerón, Rev. Sci. Instrum. **61**, 3769 (1990).

[27] D.G. Fedak and N.A. Gjostein, Surf. Sci. **8**, 77 (1967); F. Grønlund and P.E. Højlund Nielsen, J. Appl. Phys. **43**, 3919 (1972); G.K. Binnig, H. Rohrer, Ch. Gerber, and E. Stoll, Surf. Sci. **144**, 321 (1984).

[28] F. Ercolessi, E. Tosatti, and M. Parrinello, Phys. Rev. Lett. **57**, 719 (1986).

[29] O. Rodríguez de la Fuente, M.A. González, and J.M. Rojo, Surf. Sci. **454**, 16 (2000).

[30] F.R.N. Nabarro, *Theory of Crystal Dislocations* (Dover, New York, 1987), p. 89.

[31] We shall call *depression dissociation* the process by which one of the two dislocations forming a *depression* glides away from the other into a neighboring corrugation valley. The final configuration is then a pair of dislocations with $\theta \neq \pi/3$. Indeed one might

still label as a 2D dislocation dipole *any* configuration involving two 2D *interacting* dislocations of opposite Burgers vectors, independently of θ, i.e., of the orientation of the line separating them.

[32] We always carried out our irradiations on large terraces corresponding to a single domain of the Pt(001) reconstruction. We did not elucidate whether the domains on which we worked corresponded to either the so called hex or hex-$R0.7°$ reconstruction, as analyzed in Ref. 47. A detailed report of experiments on Pt will be presented elsewhere.

[33] B. Joós and M.S. Duesbery, Phys. Rev. Lett. **70**, 2754 (1993); M.S. Duesbery and B. Joós, Philos. Mag. **54**, 145 (1986); **54**, 165 (1986).

[34] G. Bilalbegović, and E. Tosatti, Phys. Rev. B **48**, 11 240 (1993); D. Passerone, F. Ercolessi, and E. Tosatti, Surf. Sci. **454**, 634 (2000).

[35] Note that a pure isotropic model would lead to the well-known result of $\theta=\pi/4$.

[36] H. Brune, H. Röder, C. Boragno, and K. Kern, Phys. Rev. B **56**, 7643 (1997); C. Günther, J. Vrijmoeth, R.Q. Hwang, and R.J. Behm, Phys. Rev. Lett. **74**, 754 (1995).

[37] C.B. Carter and R.Q. Hwang, Phys. Rev. B **51**, 4730 (1995).

[38] S. Narasimhan and D. Vanderbilt, Phys. Rev. Lett. **69**, 1564 (1993).

[39] D.R. Nelson, in *Phase Transitions* (Academic Press, London 183), 7, pp. 1–99. For a recent review see J.C. Dash, Rev. Mod. Phys. **71**, 1737 (1999); For recent calculations with a *glue* potential see F. Celestini, F. Ercolessi, and E. Tosatti, Phys. Rev. Lett. **76**, 3153 (1999).

[40] V. Fiorentini, M. Methfessel, and M. Scheffler, Phys. Rev. Lett. **71**, 1051 (1993).

[41] M. Nastasi, J.W. Mayer, and J.K. Hirvonen, *Ion-Solid Interactions* (Cambridge University Press, Cambridge 1996), Chap. 7.

[42] M. Morgenstern, and T. Michely, Philos. Mag. **79**, 775 (1999).

[43] M. Ghaly, K. Nordlund, and R.S. Averback, Philos. Mag. **79**, 795 (1999).

[44] Some preliminary results have been presented: See O. Rodríguez de la Fuente, M.A. González, and J.M. Rojo, in *Fundamental Mechanisms of Low-Energy-Beam-Modified Surface Growth and Processing*, edited by S. Moss *et al.* (MRS, Boston, 2000).

[45] S. Günther, E. Kopatzki, M.C. Bartelt, J.W. Evans, and R.J. Behm, Phys. Rev. Lett. **73**, 553 (1994); T.R. Linderoth, J.J. Mortensen, K.W. Jacobsen, E. Lægsgaard, I. Stensgaard, and F. Besenbacher, Phys. Rev. Lett. **77**, 87 (1996).

[46] In terms of fcc coordinates, and taking the topmost layer to be a (111) plane the corresponding reactions would be noted: $(a_0/4)[\bar{1}2\bar{1}]+(a_0/4)[\bar{1}01]=(a_0/2)[\bar{1},1,0]$, $(a_0/4)\times[1\bar{2}1]+(a_0/4)[10\bar{1}]=(a_0/2)[1\bar{1}0]$, where a_0 designs here the cubic cell parameter. Note that the Burgers vectors of the 2D Frank and Shockley's partial dislocations are now, respectively, of the type $(a_0/4)\langle\bar{1}2\bar{1}\rangle$ and $(a_0/4)\langle\bar{1}01\rangle$, whereas, as in the bulk $(a_0/2)\langle\bar{1}10\rangle$ is the Burgers vector of a perfect dislocation.

[47] A. Borg, A.M. Hilmen, and E. Bergene, Surf. Sci. **306**, 10 (1994).

[48] R.J. Behm, P.A. Thiel, P.R. Norton, and G. Ertl, J. Chem. Phys. **78**, 7437 (1983); A. Hopkinson, J.M. Bradley, X.C. Guo, and D.A. King, Phys. Rev. Lett. **71**, 1597 (1993).

[49] T. Michely and G. Comsa, Nucl. Instrum. Methods Phys. Res. B **82**, 207 (1993).